EPJ Web of Conferences **288**, 04007 (2023) https://doi.org/10.1051/epjconf/202328804007
*ANIMMA 2023*

# Design of an Instrumented Fuel Rod for Intra-pin Neutron Flux Measurements in the CROCUS Experimental Reactor

Tom Mager[1,*], Jean-Baptiste Valentin[1], Vincent Lamirand[1,2], Thomas Ligonnet[1], Won Dong Shin[3], Jean-Marie Fürbringer[4], Mathieu Hursin[2], Andreas Pautz[1,2]

[1]Laboratory for Reactor Physics and Systems Behaviour, Ecole Polytechnique Fédérale de Lausanne, Switzerland
[2]Nuclear Energy and Safety Research Division, Paul Scherrer Institute, Switzerland
[3]Laboratory of Intelligent Systems, Ecole Polytechnique Fédérale de Lausanne, Switzerland
[4]Section of Physics (SB SPH-GE), Ecole polytechnique Fédérale de Lausanne, Switzerland
(*) tom.mager@epfl.ch

***Abstract*—In response to the need for validating high-fidelity deterministic neutronics solvers capable of pin-resolved neutron flux distributions, an instrumented fuel rod was designed for the experimental reactor CROCUS, operated by EPFL's Laboratory for Reactor Physics and Systems Behaviour. This rod aims at obtaining intra-pin data using activation dosimetry techniques. Placed in the outer region of the reactor core, the rod utilizes spaces between four metal uranium cigars (25 cm each) to house various disk dosimeters, targeting different neutron energy ranges and allowing retrieval of radial and azimuthal intra-pin neutron reaction rates. A design of experiment (DOE) study, aided by Serpent2 Monte Carlo calculations, facilitated the selection of dosimeter material and rod design, ensuring detection of within-pin neutron flux variations while adhering to mechanical and regulatory constraints. Azimuthal divisions of activation dosimeters were irradiated at the core center and subsequently subjected to activity determination using an HPGe gamma spectrometer. The objectives were met, detecting expected azimuthal variations within dosimeters and confirming uncertainties on reconstructed activity to be smaller than the amplitude of the observed variations. A permit from the Swiss nuclear regulatory authority ENSI-IFSN was obtained, allowing installation and usage of the instrumented fuel rod in CROCUS, known as the NECTAR experiments.**

*Keywords*—**Instrumented fuel rod, Intra-pin measurements, High-fidelity, CROCUS**

## I. Introduction

In recent years, significant efforts have been devoted to advancing nuclear reactor modeling and simulation capabilities, encompassing aspects such as neutron transport, reactor thermal hydraulics, fuel performance, and material behaviors. These advancements have played a decisive role in addressing operational and safety challenges in light-water reactors, including pellet-clad interaction (PCI), departure from nucleate boiling (DNB), and corrosion product deposition (CRUD). To support these endeavors, nuclear programs worldwide have initiated the development of three-dimensional (3D) full-core time-dependent methods with pin-resolved details [1]. These high-fidelity deterministic neutronics codes can predict the steady-state neutron flux distribution directly at the pin or sub-pin scale [2]–[4], offering detailed insights into reactor behavior and performance.

However, successful utilization of such advanced modeling techniques heavily relies on the availability of high-resolution experimental data measured in a reactor. Particularly, accurate measurements of intra-pin reaction rates have been identified as crucial validation requirements for high-fidelity neutronics codes that aim to resolve local phenomena. Unfortunately, the availability of such measurements remains limited. The lack of access to locations of interest, such as within the fuel lattice and inside fuel pins, is a significant limitation for localized measurements in operating NPPs, and when such measurements exist their access is restricted. In this context, zero-power research reactors play a decisive role in generating high-quality in-core validation data. The availability and flexibility of operation in research reactors allow for investigating neutronics effects at a local scale with inter-pin and intra-pin measurements.

Some efforts have been made over the years to produce such data, including the indirect measurements of intra-pin reaction rates performed along the radial and azimuthal directions of a BWR assembly at the PROTEUS reactor of the Paul Scherrer Institute [5]. Regarding PWRs, the only available experimental intra-pin data were conducted on the IPEN/MB-01 reactor facility, where radial distributions of reaction rates were obtained from gamma ray spectroscopy and collimation techniques on irradiated fuel disk samples [6]. More recently, highly-localized inter-pin data was acquired in the CROCUS experimental reactor thanks to miniature Li-6 scintillators [7].

Despite these advancements, the validation of high-fidelity modeling codes for pin-resolved neutron flux distributions remains scarce, and to address this validation gap, the Laboratory for Reactor Physics and Systems Behavior at EPFL took the initiative to design an instrumented fuel rod for the CROCUS experimental reactor. With its double-lattice core, CROCUS poses modeling challenges, making it a demanding test for high-fidelity codes that aim to model new generations of complex cores. The instrumented fuel rod, strategically positioned in the outer region of the reactor core, is expected

to capture significant azimuthal and radial intra-pin neutron flux variations thanks to direct or indirect detection technics.

This paper presents the outcomes of an extensive design study, incorporating design of experiment (DOE) methodologies that utilize Serpent2 Monte Carlo calculations to optimize the detector system and instrumented fuel rod design. Additionally, we discuss the successful irradiation and analysis of some activation dosimeter samples with non-regular shapes at the core center of CROCUS. Finally, we present the final design of the instrumented fuel rod, for the so-called NECTAR experiments in the CROCUS zero-power reactor.

## II. Description of the Project

### A. The CROCUS Experimental Reactor

CROCUS is a zero-power research reactor located on the EPFL campus, with a maximum allowed power of 100 W. It is an ideal tool for research and education due to the acceptably low dose rates within the shielding after shutdown. The core is located in an aluminum vessel measuring 1.3 m in diameter and 1.2 cm in thickness. Demineralized light water is used as both the moderator and reflector. The active core region is cylindrical, 1 m high and approximately 60 cm in diameter, consisting of two fuel zones with square lattices of different pitches: an inner uranium oxide region containing 336 rods enriched to 1.806% with a pitch of 1.837 cm, and an outer uranium metal region with uo to 180 rods enriched to 0.947% with a pitch of 2.917 cm. The fuel loading pattern is illustrated in Fig.1.

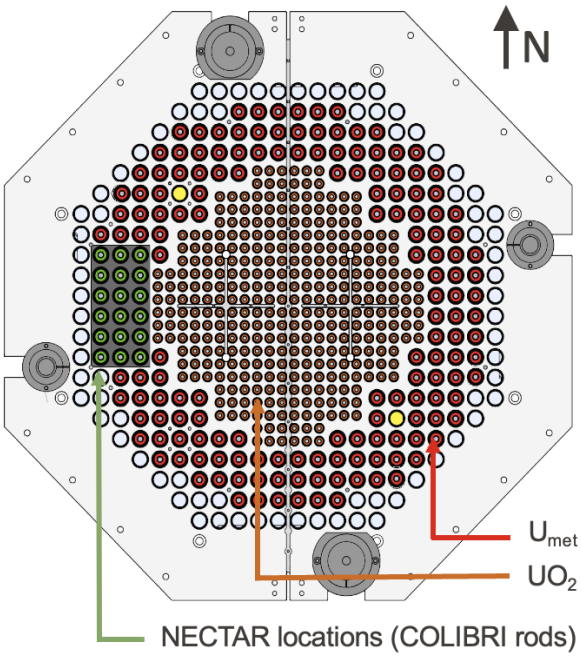


Fig. 1. CROCUS top-view of the fuel loading pattern with the two fuel lattices and the 18 locations available for the NECTAR fuel rod.

While $UO_2$ rods consist in a 1-m stack of cylindrical pellets with aluminum cladding, $U_{met}$ rods are formed of four cigars, each measuring 25 cm, also encased with aluminum. The rods are held in position by two octagonal aluminum grid plates spaced 1 meter apart. Each plate contains a 1-mm-thick cadmium layer to limit axial thermal flux and neutron doses in the reactor cavity, with the active zone of the fuel located between the two cadmium layers. Reactivity is controlled by the water level, which is controlled via a spillway, and $B_4C$ control rods.

### B. Instrumented Fuel Rod

The instrumented fuel rod will be composed of four $U_{met}$ cigars obtained from the LRS reserve, thereby positioning it in the outer core region of the reactor. To achieve intra-pin neutron flux distributions, detectors or dosimeters will be strategically placed in the space between the two central cigars. To facilitate manipulation and prevent contamination of individual cigars and dosimeters, each cigar will be individually encased. In consideration of structural integrity and water tightness, an outer cladding may be added to encompass the four cigars and the detector holder. If this arrangement is adopted, the rod will need to be positioned in the COLIBRI [8] fuel rod oscillator region (highlighted in green in Fig. 1) to take advantage of the enlarged holes in the aluminum grid plates. A representation of the potential design for the instrumented fuel rod is illustrated in Fig. 2.

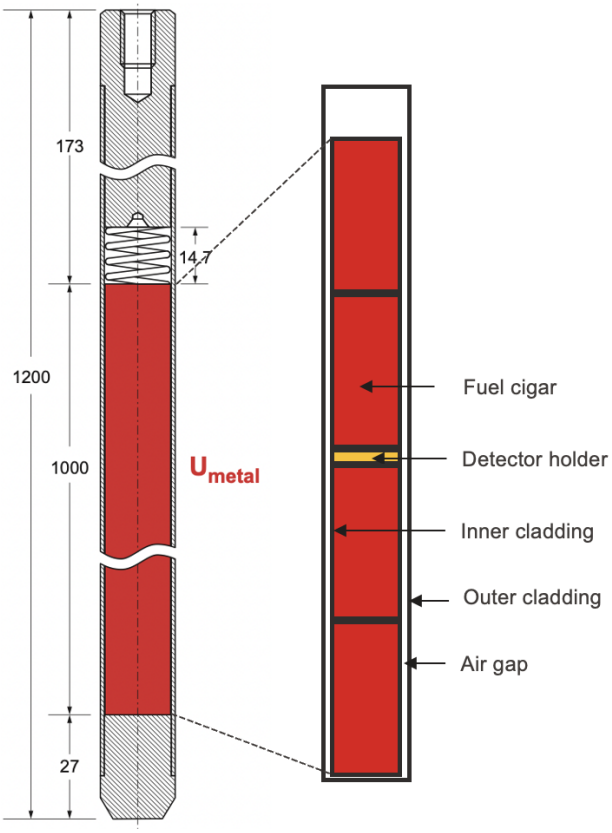


Fig. 2. Schematics of a CROCUS uranium metal fuel rod, along with a sketch of the instrumented fuel rod basic principle.

## III. Design of Experiments

In light water reactors, fission "fast" neutrons are emitted with an average energy of 2 MeV. To induce fissions again,

these neutrons need to be thermalized down to approximately 0.025 eV. Accordingly, we classify neutrons into two groups based on their energies: the ”thermal” neutrons with energies around 0.025 eV and the ”fast” neutrons with energies above the cutoff of approximately 0.625 eV. Consequently, the ”thermal” neutrons are more prevalent in the moderator surrounding fuel rods, while the ”fast” neutrons are predominantly present within the fuel. This spatial distribution results in a depression of thermal neutron flux within the fuel rod, while the fast neutron flux peaks in the fuel. These variations from the moderator to the center of the fuel rods are of particular interest for code validation purposes. Therefore, an instrumented fuel rod design that maximizes the detection of these radial variations within the fuel is desired.

To achieve this objective, we will employ Design Of Experiments (DOE) methodologies [9] to establish the relationship between the fuel rod design and the amplitude of the measured intra-pin neutron flux variations. The strategy employed is presented hereafter and will be elaborated upon in individual subsections.

**Objective:** The primary objective of this study is to design an instrumented fuel rod for the CROCUS reactor, specifically aimed at conducting precise intra-pin neutron flux measurements for the validation of high-fidelity deterministic codes. Therefore, the focus is on identifying which instrumented rod design maximizes the detection of the radial neutron flux depression within the fuel.

**Factors:** Four factors influencing the flux depression have been identified:

- the cladding material;
- the axial thickness of the inner cladding which is directly in contact with the detector holder;
- the presence or absence of an outer cladding, depending on the detector system selected;
- the detection system among gold dosimeters sensible to thermal neutrons, nickel dosimeters sensible to fast ones, or a miniature fiber-coupled scintillators developed at EPFL [10]. Dosimeter materials have been selected based on the experience gained during the PETALE program [11]–[13], the main criteria being reaction half-life, incident neutron energy and material capability for easy cutting and handling.

**Response:** Thermal and fast neutron fluxes: $^{6}$Li(n,$\alpha$), $^{197}$Au(n,$\gamma$), $^{58}$Ni(n,p) reaction rates computed with Serpent2.

**Model:** A constant coefficient model without interactions will first be considered to describe the causal relations from the factors to the response.

**Strategy:** A full factorial design could be considered, but Graeco-latin squares [14] will be used to reduce the number of Serpent2 simulations to be performed.

### A. Procedure

The stochastic Monte Carlo neutron transport code Serpent2 [15] is used to model the instrumented control rod. The model consists of a 3 by 3 arrangement of outer core fuel rods with the instrumented rod positioned at the center (Fig. 3a). Reflective boundary conditions are applied in all three dimensions. Tracklength detectors are employed to tally reaction rates along a radial traverse from the moderator to the fuel center (Fig. 3c).

For the Serpent calculations, the neutron population was set at $10^6$ neutrons per cycle, with 200 inactive followed by 10000 active cycles. Fig. 3c illustrates an example of some neutron flux profiles obtained by simulating the $^{6}$Li(n,$\alpha$) reaction detector response. A comparison is made among various axial cladding thicknesses and a reference fuel rod profile. Notably, an increase in the axial cladding thickness corresponds to a reduction in the neutron flux depression within the instrumented rod.

To evaluate the success of the simulations, the relative amplitude of the flux depression, denoted as ”r”, is used as a parameter. ”r” is defined as the ratio between the flux values at the fuel center and at the cladding internal radius. This parameter serves as a metric in assessing the accuracy of the model in capturing neutron flux variations within the fuel assembly.

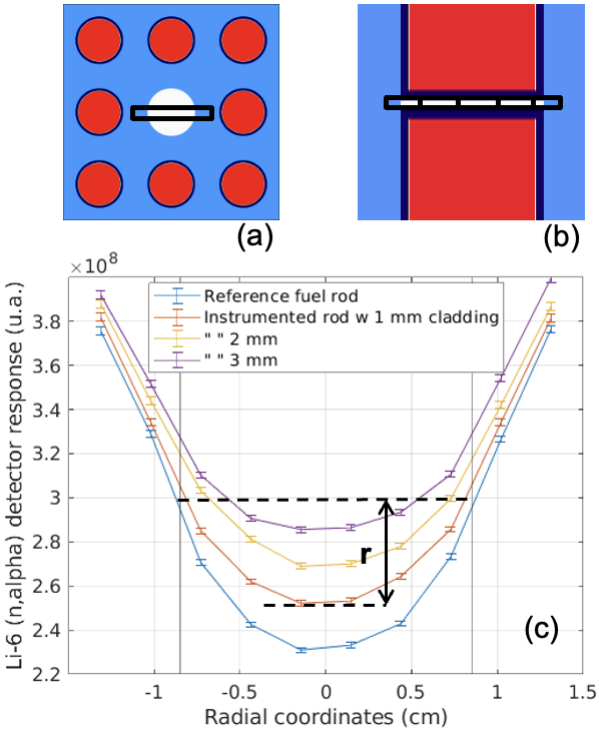


Fig. 3. (a) Axial section of the Serpent model. (b) Radial section of the instrument fuel rod with schematics of the tracklength detectors. (c) Example of Li-6 detector response distribution along the instrumented fuel rod radial profile.

### B. Matrix of Simulations

as stated previously, four factors were considered to have a possible influence on the design. The three possible levels for each factor are presented in Tab. I.

A full factorial design would necessitate 81 Serpent2 simulations, requiring extensive computation time to obtain sufficient statistics on the detector response. To address this computational burden, a Graeco-Latin square design was adopted

TABLE I
SELECTED FACTORS INFLUENCING THE DESIGN OF THE INSTRUMENTED FUEL ROD.

| **Factors** | **Levels** | | |
|---|---|---|---|
| **Axial clad thickness (mm)** | 1 | 2 | 3 |
| **Outer radial clad** | no | yes w/o air | yes w/ air |
| **Material** | Al | Zr | SS |
| **Detector** | Li-6 | Au-197 | Ni-58 |

(Tab. II), effectively reducing the simulation matrix from 81 to 9 entries.

In the Graeco-Latin square design, the axial cladding factor is represented over the rows, while the presence of outer cladding is represented over the columns. Moreover, the arrangement of materials and detectors is carefully ordered to ensure that each element of material and each element of detectors appear exactly once in every row and column, and no two cells contain the same ordered pair. This design strategy optimizes the efficiency of the simulations while maintaining a representative dataset for analysis and validation.

TABLE II
GRAECO-LATIN SQUARE DESIGN.

| | no | yes w/o air | yes w/ air |
|---|---|---|---|
| 1 mm | Al & Li-6 | Zr & Au-197 | SS & Ni-58 |
| 2 mm | Zr & Ni-58 | SS & Li-6 | Al & Au-197 |
| 3 mm | SS & Au-197 | Al & Ni-58 | Zr & Li-6 |

Instead of tallying just one detector response per case, we made modifications to the Serpent 2 inputs, enabling us to obtain three virtual detector responses for each configuration. Detectors were therefore not explicitly modeled. As a result, we were able to generate an extended dataset consisting of 27 simulations. To organize these simulations efficiently, they can be grouped into three Graeco-Latin squares, mirroring the format of the initial set of 9 simulations (Tab. III). The first three rows represent the first set of 9 simulations, while the 6 additional rows were obtained by conducting permutations over the three detector levels.

TABLE III
GRAECO-LATIN SQUARE DESIGN.

| | no | yes w/o air | yes w/ air |
|---|---|---|---|
| 1 mm | Al & Li-6 | Zr & Au-197 | SS & Ni-58 |
| 2 mm | Zr & Ni-58 | SS & Li-6 | Al & Au-197 |
| 3 mm | SS & Au-197 | Al & Ni-58 | Zr & Li-6 |
| 1 mm | Al & Au-197 | Zr & Ni-58 | SS & Li-6 |
| 2 mm | Zr & Li-6 | SS & Au-197 | Al & Ni-58 |
| 3 mm | SS & Ni-58 | Al & Li-6 | Zr & Au-197 |
| 1 mm | Al & Ni-58 | Zr & Li-6 | SS & Au-197 |
| 2 mm | Zr & Au-197 | SS & Ni-58 | Al & Li-6 |
| 3 mm | SS & Li-6 | Al & Au-197 | Zr & Ni-58 |

### C. Model

In DOE, constant coefficient models, also known as simple linear models, are often employed to approximate the relationship between factors and the response variable [14]. This type of models assumes that the effects of the factors are constant across the entire experimental domain. They are relatively simple and easy to interpret, especially when dealing with a small number of factors. The experimental design and data analysis process is easy to implement as the assumption of linearity allows the use of standard linear regression techniques for parameter estimation. Utilizing a simple model facilitates the identification and interpretation of significant effects of the factors on the response variable. However, constant coefficient models may not accurately capture complex relationships between factors and the response variable, especially in cases where the true relationship is nonlinear or contains interactions between factors. Constant coefficient models are also not suitable for extrapolation beyond the range of the experimental data.

Although we have interaction between factors, especially between the choice of detector and the presence of an outer cladding, we started our analysis with the following constant coefficient model for the sake of simplicity:

$$r_{otmd} = \mu + \gamma_{oc} + \tau_{thick} + \omega_{mat} + \zeta_{det} + \epsilon \qquad (1)$$

where $r_{otmd}$ represents the relative amplitude of the flux depression that we want to maximize, $\mu$ is the total average of the simulations, $\gamma$, $\tau$, $\omega$ and $\zeta$ are respectively the effects of the four considered factors $oc$: outer cladding, $thick$: cladding thickness, $mat$: material and $det$: detectors. The residuals are considered in the coefficient $\epsilon$. For each of the 27 configurations described in Tab. II, the simulated relative amplitude of the detector response depression $r_{otmd}$ observed between the fuel center and its boundary has been reported in Tab. IV.

TABLE IV
RELATIVE AMPLITUDE OF THE DETECTOR RESPONSE DEPRESSION (%).

| | no | yes wo air | yes w air |
|---|---|---|---|
| 1 mm | 11.53 ± 0.098 | 4.7 ± 0.16 | 5.32 ± 0.14 |
| 2 mm | 8.38 ± 0.11 | 14.90 ± 0.19 | 3.28 ± 0.11 |
| 3 mm | 9.04 ± 0.038 | 5.99 ± 0.0081 | 6.63 ± 0.0055 |
| 1 mm | 3.46 ± 0.16 | 8.05 ± 0.22 | 16.64 ± 0.11 |
| 2 mm | 9.72 ± 0.0079 | 7.93 ± 0.42 | 4.49 ± 0.0058 |
| 3 mm | 3.81 ± 0.0053 | 4.97 ± 0.0040 | 4.10 ± 0.019 |
| 1 mm | 9.99 ± 0.14 | 10.27 ± 0.0080 | 8.42 ± 0.47 |
| 2 mm | 4.27 ± 0.19 | 4.59 ± 0.15 | 7.82 ± 0.0063 |
| 3 mm | 19.12 ± 0.0017 | 2.03 ± 0.0090 | 4.05 ± 0.0053 |

From this set of 27 simulations, we were able to extract the constant coefficients displayed in Eq. 2.

$$\widehat{r_{otmd}} \approx 7.54 + \underbrace{\begin{Bmatrix} 1.27 \\ -0.49 \\ -0.79 \end{Bmatrix}_{oc}}_{} + \underbrace{\begin{Bmatrix} 1.17 \\ -0.27 \\ -0.90 \end{Bmatrix}_{thick}}_{} + \underbrace{\begin{Bmatrix} -1.59 \\ -0.85 \\ 2.44 \end{Bmatrix}_{mat}}_{} + \underbrace{\begin{Bmatrix} 3.75 \\ -2.29 \\ -1.46 \end{Bmatrix}_{det}}_{} \qquad (2)$$

Fig. 4 provides a visual representation of the effect of each factor, helping the reader in better understanding their impact. The centerline, depicting a 0% effect, represents the

average response of the 27 simulations. As our objective is to identify the optimal design maximizing the detector response depression, it is crucial to focus on the levels with higher effects. Notably, the selection of the detector and cladding material holds greater importance than the thickness of the axial cladding and the presence of an outer cladding.

The n-way analysis of variance (ANOVAN) in Fig. 5 further supports this observation, revealing that the p-values for the factors corresponding to material and detector are both lower than 0.05. Hence, these two factors are the only ones with a statistically significant effect, representing a 5% risk of concluding that an effect exists when, in reality, there is no actual effect.

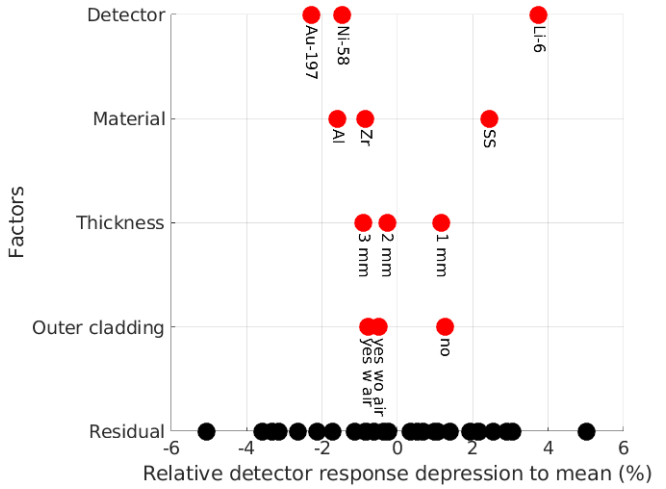


Fig. 4. Effects of each factor's level on the detector response depression in the fuel.

| Source | Sum Sq. | d.f. | Mean Sq. | F | Prob>F |
|---|---|---|---|---|---|
| Outer cladding | 22.39 | 2 | 11.1948 | 1.38 | 0.276 |
| Thickness | 20.306 | 2 | 10.1529 | 1.26 | 0.3088 |
| Material | 82.63 | 2 | 41.3151 | 5.11 | 0.0175 |
| Detector | 193.106 | 2 | 96.5532 | 11.94 | 0.0005 |
| Error | 145.6 | 18 | 8.0889 | | |
| Total | 464.032 | 26 | | | |

Fig. 5. N-way analysis of variance (ANOVAN).

### *D. Discussion*

Based on the constant coefficient model and its analysis of variance, the choice of the detection system and the cladding material appears to be the only factors significantly impacting the response. Initially, the seemingly favorable solution for the instrumented rod design would involve a single stainless steel cladding with an axial thickness of 1 mm, coupled with Li-6 scintillators as the detection system. However, it is important to consider that Li-6 scintillators are connected to optical fibers, requiring the presence of an outer cladding with sufficient space to accommodate them from the center of the fuel rod to the acquisition system. Consequently, the level of the "outer cladding" factor will be set to "yes w/space," with little impact on the response, as evident from the ANOVAN results.

Another material constraint is the choice of cladding material. Despite stainless steel being the optimal choice, Al-6060 has been selected to ensure compatibility with all CROCUS internals, leveraging our workshop's expertise, and simplifying the process of obtaining a permit from the Swiss regulator, ENSI.

As a result, the instrumented fuel rod will be produced using Al-6060, featuring the smallest possible inner cladding axial thickness and an outer cladding. With these design choices, the constant coefficient model predicts the radial reaction rate depression within the fuel to be 10.11$\pm$ 0.13% with Li-6 scintillators, 4.9 $\pm$ 0.21% with Ni-58 dosimeters, and 4.0 $\pm$ 0.23% with gold dosimeters. In order to check the validity of the model, we proposed to fix 3 factors arbitrarily and to run simulations on the 3 levels of the last one. We therefore fixed the outer cladding on "yes w/ space", the thickness on "1 mm", the material on "Aluminum", and we ran 3 simulations varying the detector on "Li-6", "Au-197" and "Ni-58". Relative errors between the flux depressions predicted by the model and the simulated ones are respectively 13, 21 and 23%. However, these first estimates offer valuable insights into the expected performance of the instrumented fuel rod under various conditions and highlight the importance of appropriate material selection and detector system in achieving the desired response. A DOE model taking interactions between factors into account would be needed to improve our predictions.

## IV. The Instrumented Fuel Rod

Considering the results of the Design of Experiments (DOE) and the various constraints presented in Section III-D, the following design for the instrumented rod was adopted and submitted to the Swiss nuclear regulatory authority ENSI-IFSN for examination, with the goal of obtaining a permit for the installation and usage of the rod in CROCUS.

The instrumented rod, which can be placed alternatively in one of the 18 COLIBRI slots (see Fig. 1), taking the position of the existing rod at the desired measurement location, is constructed as follows (refer to Fig. 6):

The rod comprises four $U_{met}$ fuel cigars from the LRS reserve. These cigars are identical to those used in CROCUS $U_{met}$ rods and are enriched to 0.947% in $^{235}$U. Each cigar measures 25 cm in length and has a diameter of 17 mm. They are individually clad with an Al-6060 sheath, sealed using O-rings with a thickness of 1.5 mm, resulting in an outer diameter of 20.3 mm.

An Al-6060 outer sheath with a 22 mm internal diameter and a 25 mm external diameter forms the second layer. This layer has a wall thickness of 1.5 mm and is sealed with an aluminum plug screwed at its lower end, ensuring its tightness with an O-ring. The plug also serves as a centering piece in the lower grid.

Centering devices for dosimeters are placed between each clad cigar, enabling precise and reproducible positioning in terms of centering, height, and angle.

A fixing piece is attached to the upper end of the outer sheath, facilitating the manual or remote retrieval of the rod. At the upper part, the instrumented rod is positioned using a

centering piece fixed in the passage hole of the upper grid and the moving plate of COLIBRI.

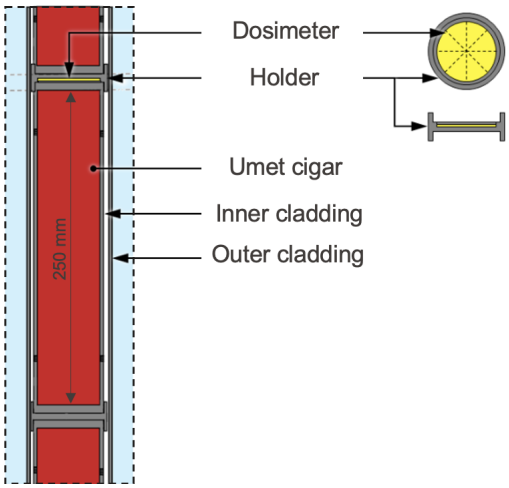


Fig. 6. Schematic diagram of the NECTAR instrumented fuel rod.

## V. Dosimetry Testing

The last step in the design process involves conducting reactor dosimetry testing to verify the observation of reaction rate variations within dosimeters. For this purpose, nickel dosimeters with azimuthal sections are irradiated at the core center of CROCUS, with two distinct objectives in mind. Firstly, this testing aims to gain experience in HPGe gamma spectroscopy measurement and post-processing techniques. Secondly, it seeks to demonstrate the detection of neutron flux variations within pin-size dosimeters and to estimate experimental uncertainties.

The nickel dosimeter, measuring 17.3 mm in diameter and 0.5 mm in thickness, will feature 8 azimuthal sections and will be placed at the CROCUS core center, as schematically shown in Fig. 7a. Upon irradiation, the $^{58}$Ni(n,p) reaction will produce for one third $^{58}$Co$^{m}$ with a half-life of 9.04 hours and for two thirds $^{58}$Co, which, through electron capture, will yield $^{58}$Fe with a half-life of 70.86 days [16]. To ensure sufficient counts, the dosimeter will be irradiated at 60 W for 1 hour, aiming for at least 80000 counts per section for the 811 keV gamma peak of the $^{58}$Ni(n,p)$^{58}$Co reaction, which will be measured using the LRS high-efficiency gamma-ray spectrometer.

Post-irradiation, a waiting period of 4 days is required to allow the quantity of parasitic $^{58}$Co$^{m}$ in the dosimeter to decrease to a negligible amount.

The full nickel dosimeter activity was initially measured before being cut into its 8 azimuthal sections. As shown in Fig. 7b, the specific activity of each of the 8 azimuthal sections is compared to the activity of the full dosimeter measured before cutting. As expected, the mass-weighted average of the 8 slices matches the full dosimeter's activity, serving as proof of principle for the observation of neutron flux variations within the dosimeter.

The two-sigma error bars encompass uncertainties related to statistics, HPGe efficiency at 810 keV, $^{58}$Co gamma emission probability, auto-absorption, and activation cross-section. The uncertainty on the detector efficiency at 810 keV was determined by the efficiency calibration of the HPGe spectrometer. The $^{58}$Co gamma emission probability is known from literature [16]. The activation cross-section along with its uncertainty was computed from IRDFF microscopic cross section data [17] and neutron flux tallied in the dosimeter with Serpent2 simulations. Auto-absorption probability and respective uncertainty were retrieved from Serpent2 simulations with point source and exact detector geometry.

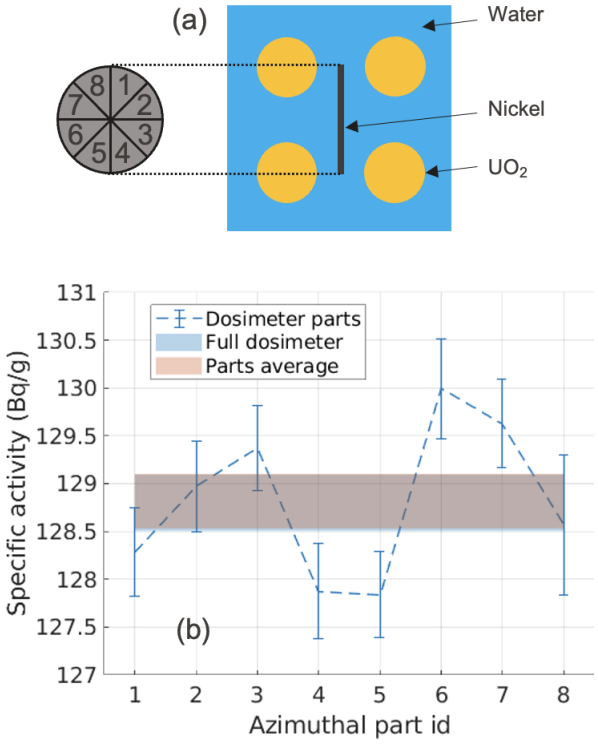


Fig. 7. (a) Schematics of the irradiation location. (b)Mass weighted activity of the dosimeters.

Regarding the azimuthal variations, it can be observed that sections 2, 3, 6, and 7, which are closer to the fuel pins, exhibit higher specific activities compared to the other sections. This outcome confirms our capability to detect azimuthal neutron flux variations within the dosimeter, as $^{58}$Ni is more sensitive to fast neutrons, which are more abundant in the fuel than in the moderator. However, the maximum relative amplitude of these variations is only 1.7%. While uncertainties on HPGe efficiency at 810 keV, $^{58}$Co gamma emission probability, auto-absorption, and activation cross-section are correlated from one section of dosimeter to the other, the primary contributor to the error bars is the counting uncertainty, which could be mitigated through higher power irradiation and longer HPGe times, while respecting to the power limit authorization of 100 W.

The observed 1.7% amplitude falls below the 4% predicted by the constant coefficient model for within-pin variations, which can be attributed to the fuel pins' fast neutron flux distribution differing from that in the moderator region.

## VI. Conclusion

In this study, we successfully designed and manufactured an instrumented fuel rod tailored for intra-pin neutron flux measurements within the CROCUS reactor. Employing design of experiments (DOE) methodologies, we systematically investigated the key parameters affecting our response, specifically the amplitude of neutron flux variations within the fuel pin. The constant coefficient model used and its analysis of variance revealed that the choice of cladding material and detection system were the primary factors influencing the observed response.

Adhering to safety and regulatory constraints, we were constrained in our selection of cladding material, leading us to opt for Al-6060. To maximize data acquisition capabilities, we incorporated multiple detection systems, including Li-6 scintillators, Ni-58, and Au-197 dosimeters. The DOE study highlighted Li-6 fiber-coupled scintillators as the most favorable detection system, but considering practical aspects, we conducted reactor dosimetry testing with Nickel scintillators. The results confirmed that our design enabled the observation of within-pin variations, although with smaller amplitudes compared to Li-6.

In light of the testing outcomes and to ensure future flexibility, we prioritized the use of dosimeters while ensuring our design could accommodate fiber-coupled Li-6 scintillators when suitable. In parallel, we sought and successfully obtained a permit from the Swiss nuclear regulatory authority ENSI-IFSN, authorizing the installation and operation of the instrumented fuel rod in the CROCUS reactor.

Standing as the second intrapin neutron flux measurements in a LWR performed worlwide, this experiment should yield rare and highly valuable data. Our primary objective is to complement the existing CROCUS IRPhE benchmark in order to make the experimental dataset available to the community and facilitate high-fidelity neutronics solver validation.

## Acknowledgment

I would like to express my sincere gratitude to the mechanics from the EPFL workshops, who played indispensable roles in the design, testing and development, of the instrumented fuel rod for the CROCUS nuclear reactor. Their unwavering support and expertise were essential throughout the entire project.
I extend my heartfelt thanks to:

- Gilles Grandjean, the workshop supervisor, for his essential guidance and initial assistance in getting started with the design of the instrumented fuel rod.
- Daniel Clément and Luc Chevalley, for their invaluable contributions in producing the first prototypes and conducting the crucial initial tests.
- Virgile Cavin, for his dedication and skill in overseeing the entire production process of the fuel rod, ensuring its successful realization.
- Claude Amendola, responsible for the production and laser pre-cut of dosimeters, a critical component of the rod.
- Daniel Godat, our lab mechanics, who provided great support in the final adjustments to ease handling and integration of the rod into the reactor core.

This project would not have been possible without their remarkable collective efforts and commitment.

## References

[1] P. J. Turinsky and D. B. Kothe, "Modeling and simulation challenges pursued by the consortium for advanced simulation of light water reactors (CASL)," *Journal of Computational Physics*, vol. 313, pp. 367–376, may 2016.
[2] MPACT Team, "MPACT Theory Manual," Oak Ridge National Laboratory, Technical Report CASL-U-2019-1874-001, November 2019.
[3] N. Choi, H. Park, H. G. Lee, S. Jae, S. Jeon, and H. G. Joo, "Recent capability and performance enhancements of the whole-core transport code ntracer." *EPJ Web of Conferences*, vol. 247, p. 06033, 2021.
[4] T. Mager, M. Hursin, C. Fiorina, and A. Pautz, "Development of a high fidelity model of the crocus experimental reactor," in *PHYSOR 2022 - International Conference on physics of reactors.*, 05 2022.
[5] K. Macku, F. Jatuff, M. Murphy, M. Plaschy, P. Grimm, O. P. Joneja, and R. Chawla, "Radial and azimuthal 235u fission and 238u capture distributions in BWR UO2 pins: CASMO-4 and MCNP4c versus activation foil measurements," *Nuclear Science and Engineering*, vol. 155, no. 1, pp. 96–101, jan 2007.
[6] A. D. Santos, *U(n,f) and 238 U(n,gamma) Reaction Rates Across the Fuel Pellet Radius of the IPEN/MB-01 Reactor,*. International Handbook of Evaluated Reactor Physics Benchmark Experiments, NEA/NSC/DOC/(2006)1, Organisation for Economic Co-operation and Development, Nuclear Energy Agency, 2018, ch. IPEN(MB01)-LWR-RESR-019.
[7] F. Vitullo, "Miniature and minimalistic neutron detectors for online high-resolution experiments in the zero-power reactor crocus," p. 171, 2022. [Online]. Available: http://infoscience.epfl.ch/record/296483
[8] V. Lamirand, P. Frajtag, D. Godat, O. Pakari, A. Laureau, A. Rais, M. Hursin, G. Hursin, C. Fiorina, and A. Pautz, "The colibri experimental program in the crocus reactor: characterization of the fuel rods oscillator," *EPJ Web of Conferences*, vol. 225, p. 04020, 01 2020.
[9] G. E. P. Box, W. G. Hunter, and J. S. Hunter, *Statistics for Experimenters: Design, Innovation, and Discovery*, 2nd ed. Wiley-Interscience, 2005.
[10] F. Vitullo, V. Lamirand, J.-B. Mosset, P. Frajtag, O. Pakari, G. Perret, and A. Pautz, "A mm3 fiber-coupled scintillator for in-core thermal neutron detection in crocus," *IEEE Transactions on Nuclear Science*, vol. 67, no. 4, pp. 625–635, apr 2020.
[11] A. Laureau, A. Gruel, V. Lamirand, T. Ligonnet, A. Sardet, and A. Pautz, "Analysis of the preliminary campaign for the petale program," *EPJ Nuclear Sciences Technologies*, vol. 9, 06 2023.
[12] Lamirand, Vincent, Laureau, Axel, Rochman, Dimitri, Perret, Gregory, Gruel, Adrien, Leconte, Pierre, Blaise, Patrick, and Pautz, Andreas, "An experimental programme optimized with uncertainty propagation: Petale in the crocus reactor," *EPJ Web Conf.*, vol. 211, p. 03003, 2019. [Online]. Available: https://doi.org/10.1051/epjconf/201921103003
[13] T. Ligonnet, "Preliminary analysis of the petale program and comparison to simulations," p. 85, 2021. [Online]. Available: http://infoscience.epfl.ch/record/289130
[14] D. Montgomery and C. St, *Design and Analysis of Experiments, 9th Edition*, 07 2022.
[15] J. Leppanen, "Development of a new monte carlo reactor physics code," *978-951-38-7018-8*, 2007.
[16] W. C. Morgan, "Long-term neutron activation products of nickel-58." [Online]. Available: https://www.osti.gov/biblio/10172408
[17] A. Trkov, P. Griffin, S. Simakov, L. Greenwood, K. Zolotarev, R. Capote, D. Aldama, V. Chechev, C. Destouches, A. Kahler, C. Konno, M. Koštál, M. Majerle, E. Malambu, M. Ohta, V. Pronyaev, V. Radulović, S. Sato, M. Schulc, E. Šimečková, I. Vavtar, J. Wagemans, M. White, and H. Yashima, "Irdff-ii: A new neutron metrology library," *Nuclear Data Sheets*, vol. 163, pp. 1–108, 2020. [Online]. Available: https://www.sciencedirect.com/science/article/pii/S0090375219300687